LIMNOLOGY and OCEANOGRAPHY

ASLO

Limnol. Oceanogr. 67, 2022, 2140–2156

doi: 10.1002/lno.12194

Stable isotopes of nitrate record effects of the 2015–2016 El Niño and diatom iron limitation on nitrogen cycling in the eastern North Pacific Ocean

Margot E. White,[1*,a] **Patrick A. Rafter**,[2] **Brandon M. Stephens**,[3] **Matthew R. Mazloff**,[1] **Scott D. Wankel**,[4] **Lihini I. Aluwihare**[1]

[1]Scripps Institution of Oceanography, University of California, San Diego, California
[2]University of California, Irvine, California
[3]University of California, Santa Barbara, California
[4]Woods Hole Oceanographic Institution, Woods Hole, Massachusetts

Abstract

In eastern boundary current systems, strong coastal upwelling brings deep, nutrient-rich waters to the surface ocean, supporting a productive food web. The nitrate load in water masses that supply the region can be impacted by a variety of climate-related processes that subsequently modulate primary productivity. In this study, two coastal upwelling regimes along central and southern California were sampled seasonally for nitrogen and oxygen stable isotopes of nitrate (i.e., nitrate isotopes) over several years (2010–2016) on 14 California Cooperative Oceanic Fisheries Investigations (CalCOFI) cruises. Seasonal, interannual, and spatial variations in euphotic zone nitrate isotopes were largely driven by the extent of nitrate utilization, sometimes linked to iron limitation of diatom productivity. Pronounced isotopic enrichment developed with the El Niño conditions in late 2015 and early 2016 which likely resulted from increased nitrate utilization linked to reduced nitrate supply to the euphotic zone. Differential enrichment of nitrogen and oxygen isotopes was observed in the surface ocean, suggesting that phytoplankton increased their reliance on locally nitrified (recycled) nitrate during warmer and more stratified periods. Overall, nitrate isotopes effectively differentiated important euphotic zone processes such as nitrate assimilation and nitrification, while archiving the influence of disparate controls such as iron limitation and climatic events through their effects on nitrate utilization and isotopic fractionation.

In the eastern North Pacific Ocean's southern California Current System (CCS), spring and summertime wind-driven upwelling of nutrient-rich waters sustains high levels of phytoplankton growth, which supports a productive ecosystem typical of eastern boundary current systems worldwide (Chan et al. 2008). The California Cooperative Oceanic Fisheries Investigation (CalCOFI) survey was established in the late 1940s to examine fluctuations in commercially important planktivorous fish populations in the CCS region, as well as the bottom-up controls on phytoplankton productivity that ultimately support these fisheries (McClatchie 2014). The spatial extent of the survey and the measurements made on its quarterly cruises have evolved over the decades, but since the early 1980s, a core group of physical, chemical, and biological measurements has been maintained, providing a rich time series of the climatology and biogeochemistry of the region (www.calcofi.org).

Data from the CalCOFI time series have demonstrated the central role of nitrate (NO_3^-) in maintaining the food web (Mantyla et al. 2007; Stukel et al. 2011; Brzezinski et al. 2015). Measurements of long-term NO_3^- variability, expressed in various ways including the nitracline depth (Aksnes and Ohman 2009) and NO_3^- concentration in upwelling source waters (Eppley and Peterson 1979; Stephens et al. 2018) have shown that chlorophyll *a* (Chl *a*) concentrations are controlled by NO_3^- delivery. The flux of NO_3^- into the euphotic zone is in turn modulated by the regional climate state. This state can vary substantially and is strongly influenced by the El Niño Southern Oscillation (ENSO) climate mode (Kahru et al. 2009; Bograd et al. 2015; Jacox et al. 2016).

*Correspondence: mew070@ucsd.edu

Additional Supporting Information may be found in the online version of this article.

[a]Present address: Department of Earth Sciences, ETH Zurich, Zurich, Switzerland

Author Contribution Statement: P.A.R. ran samples from 2010 to 2012. M.E.W. and S.D.W. ran samples from 2013 to 2016. M.E.W. analyzed the data. B.M.S. provided important feedback. M.R.M. provided modeling data and helpful discussions. M.E.W. and L.I.A. wrote the manuscript.

El Niño events (the positive ENSO phase) lead to anomalously warm sea surface temperatures in the tropical Pacific and influence the CCS via altered atmospheric circulation and ocean advection (Frischknecht et al. 2015). Atmospheric heat transport warms the surface layer and stratifies the upper ocean, reducing vertical transport along the coast of central and southern California. Meanwhile, poleward ocean heat advection from coastally trapped waves originating in the tropical Pacific brings anomalously warm and saline subtropical water into the CCS at depths below the surface, depressing the pycnocline (Jacox et al. 2015). All of these mechanisms can impact the quantity of NO_3^- delivered to the euphotic zone and thus primary production (Lilly et al. 2019).

Nitrogen isotopes of archived zooplankton and sedimentary organic N have been used to provide insight into long-term variations in the source characteristics and utilization of NO_3^- upwelling into the euphotic zone, and further show that N supply in the CCS is sensitive to climate variability such as ENSO (Ohman et al. 2012; Décima et al. 2013; Tems et al. 2015). For isotope measurements, delta notation is used to describe the isotopic composition of a sample relative to a standard and is expressed in units of permil (‰), where $\delta = [(R_{Sample}/R_{Standard}) - 1] \times 1000$ and R is the ratio of the heavy (^{15}N or ^{18}O) to the light (^{14}N or ^{16}O) isotope. N isotope measurements are standardized to atmospheric N_2 and O isotope measurements are standardized to Vienna Standard Mean Ocean Water (McIlvin and Casciotti 2011; Weigand et al. 2016). Studies have found that nitrogen isotopes ($\delta^{15}N$) of zooplankton in the CalCOFI region were significantly elevated during El Niño events compared to the long-term average (Rau et al. 2003; Ohman et al. 2012; Décima et al. 2013). Such an enrichment could result from a decrease in the supply of NO_3^-, an increase in the proportion of NO_3^- utilized (regardless of supply), a change in the isotopic composition of the source NO_3^-, and/or a shift in trophic position. Sediment trap studies also identified an increase in the $\delta^{15}N$ of organic N in sinking particles during the 2015–2016 El Niño (Davis et al. 2019). In this region, such trends have previously been attributed to a change in the $\delta^{15}N$ value of NO_3^- fueling organic matter production in the surface ocean (Castro et al. 2001; Tems et al. 2015). However, such an enrichment could also result from more complete NO_3^- utilization in the euphotic zone with no change in the $\delta^{15}N$ value of source NO_3^- (Altabet 1988).

In order to explicitly examine the influence of ENSO on nitrate sources and cycling in the region and to provide a framework for interpreting N isotopes in sedimentary and archived biological reservoirs, we conducted the first large-scale analysis of water column nitrate isotopes collected on CalCOFI cruises. In this study, we measured $\delta^{15}N$ and $\delta^{18}O$ of NO_3^- ($\delta^{15}N_{NO3}$ and $\delta^{18}O_{NO3}$) along two CalCOFI lines (Fig. 1): Line 80.0 (hereafter referred to as the northern line) off the coast of central California, where coastal upwelling is consistently observed in the spring and summer and which supports a diatom-based food web with some of the highest primary production observed within the modern CalCOFI grid; and Line 93.3 (hereafter referred to as the southern line) off the coast of southern California, where upwelling is more intermittent and primary productivity is sometimes limited by lower iron concentrations (King and Barbeau 2007). By considering these two sampling lines within CalCOFI, we were able to study two different regimes and their response to the El Niño event of 2015–2016. The extent of NO_3^- consumption strongly impacted temporal and spatial variability in NO_3^- isotopes, and other parameters measured during CalCOFI cruises illuminated potential controls on the degree of NO_3^- utilization. Nitrate-$\delta^{15}N$ and -$\delta^{18}O$ together also provided unique insights into N transformation processes in the euphotic zone whose relative importance could not be determined from measuring standing stocks of N alone.

Materials and methods

Sample collection

Samples for NO_3^- isotope analysis were collected from Lines 80.0 and 93.3 of the CalCOFI grid (Fig. 1, http://calcofi.org). Most measurements came from Stas. 93.30 to 93.60 and 80.55 to 80.80. These inshore stations exhibit greater temporal variability of biogeochemical parameters and experience greater wind-driven upwelling compared to the more offshore stations (*see* Supplementary Table S1 for a complete list of locations and time periods sampled). Samples from ≤ 150 m were analyzed from 14 CalCOFI cruises from 2010 to 2016 (Fig. 2). Samples for NO_3^- isotopes were filtered through GF/F filters (0.7-μm pore size) directly from Niskin bottles mounted on a standard conductivity-temperature-depth rosette system and frozen until analysis.

Nutrient concentrations and isotope analyses

Ancillary data were collected, analyzed, and made publicly available through the CalCOFI program (http://calcofi.org/data.html). Accuracy for NO_3^- concentrations was 0.05 μmol L^{-1} based on measurement of standards. Instrument precision was 0.01 μmol L^{-1} and the detection limit for $NO_3^- + NO_2^-$ was 0.02 μmol L^{-1}. $\delta^{15}N_{NO3}$ and $\delta^{18}O_{NO3}$ were analyzed using the denitrifier method (Sigman et al. 2001; Casciotti et al. 2002; McIlvin and Casciotti 2011; Weigand et al. 2016), in which denitrifying bacteria quantitatively convert NO_3^- to N_2O for isotopic analysis. Samples from 2010 to 2012 were analyzed at Princeton University with N_2O purification on a custom-built purge and trap system and subsequent measurement on a Thermo-Finnigan Delta Plus or MAT253 IRMS. NO_2^- was removed from all samples with measurable NO_2^- concentrations by addition of sulfamic acid prior to injection (Granger and Sigman 2009). All corrections for drift, size, and fractionation of N and O isotopes during bacterial conversion were accomplished using NO_3^- reference materials IAEA-N3, USGS 32, and USGS 34 (Böhlke et al. 2003; Brand

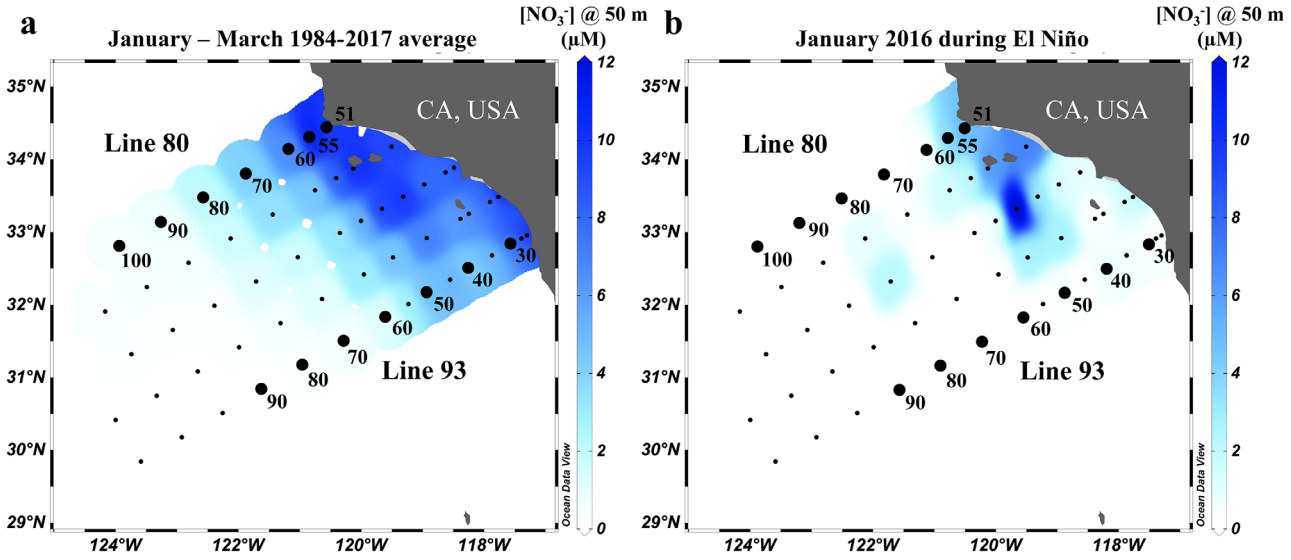

FIG. 1. Locations of CalCOFI stations sampled for NO_3^- isotopes in this study—Line 80.0 off Point Conception (northern line) and Line 93.3 off San Diego (southern line). Black circles show all regularly sampled CalCOFI stations and those sampled in this study are labeled with station numbers. (**a**) The 1984–2017 average NO_3^- concentrations at 50 m in winter (January to March) highlight the north–south and inshore–offshore gradients in NO_3^- concentration. (**b**) The NO_3^- concentrations at 50 m for winter 2016 during the El Niño event show that NO_3^- concentrations along both lines were much lower during the El Niño compared to the seasonal average. See Supplementary Table S1 for a complete list of locations and time periods covered by this data set as well as seasonal designations.

et al. 2009; McIlvin and Casciotti 2011). An overall analytical accuracy of ± 0.2 ‰ for $\delta^{15}N_{NO3}$ and ± 0.3 ‰ for $\delta^{18}O_{NO3}$ is based on all measurements of the seawater based, in-house standard included in every batch of analyses. Replicate measurements were done for 120 out of 301 $\delta^{15}N_{NO3}$ samples (triplicates or greater [$n = 37$]) and 40 out of 283 $\delta^{18}O_{NO3}$ samples (triplicates or greater [$n = 6$]). For $\delta^{15}N_{NO3}$ the analytical error ranged from 0.0005 to 2.47 ‰ with a median value of 0.05 ‰. For $\delta^{18}O_{NO3}$, the analytical error ranged from 0.0047 to 0.425 ‰ with a median value of 0.06 ‰.

Samples from 2013 to 2016 were analyzed at Woods Hole Oceanographic Institution. Briefly, sample N_2O was purified using a customized purge and trap system and analyzed on a continuous flow IsoPrime 100 isotope ratio mass spectrometer (IRMS). NO_2^- concentrations greater than 2% of NO_3^- + NO_2^- were removed by addition of sulfamic acid prior to injection (Granger and Sigman 2009). Corrections for drift, size, and fractionation of O isotopes during bacterial conversion were carried out using NO_3^- reference materials USGS 32, USGS 34, and USGS 35 (Böhlke et al. 2003; Brand et al. 2009; McIlvin and Casciotti 2011). Of 242 samples, 176 were measured in replicate (triplicates or greater [$n = 69$]) for $\delta^{15}N_{NO3}$ and 173 (triplicates or greater [$n = 76$]) out of 242 for $\delta^{18}O_{NO3}$. The analytical error for $\delta^{15}N_{NO3}$ ranged from 0.01 to 1.43 ‰ with a median value of 0.36 ‰. For $\delta^{18}O_{NO3}$, the analytical error ranged from 0.01 to 0.99 ‰ with a median value of 0.31 ‰. Although lower concentrations of NO_3^- in the sample can lead to greater error, no relationship was found between [NO_3^-] and measured error for either $\delta^{15}N_{NO3}$ or $\delta^{18}O_{NO3}$. For samples without an associated analytical error, the median value for that dataset was used to propagate error in further calculations.

Estimating nitrate uptake isotope effects

The relative strength of isotopic discrimination is represented by the isotope effect and is expressed in permil (‰) as ε (where $\varepsilon = [1 - (k^{heavy}/k^{light})] \times 1000$, and k represents the rate constant of the heavy or light isotope, respectively). Nitrogen isotope effects ($^{15}\varepsilon$) for NO_3^- uptake by phytoplankton were calculated by fitting both open and closed system Rayleigh fractionation models. The closed system model is described as

$$\delta^{15}N_{NO3} = \delta^{15}N_{NO3,initial} - {}^{15}\varepsilon \times \ln\left(\frac{[NO_3^-]}{[NO_3^-]_{initial}}\right) \quad (1)$$

The open system model, where new NO_3^- is supplied continuously, is described by the following equation

$$\delta^{15}N_{NO3} = \delta^{15}N_{NO3,initial} + {}^{15}\varepsilon \times \left(1 - \frac{[NO_3^-]}{[NO_3^-]_{initial}}\right) \quad (2)$$

where $\delta^{15}N_{NO3,initial}$ and $[NO_3^-]_{initial}$ refer to immediate source waters to the euphotic zone, the determination of which is described below. Each profile was individually evaluated using both models. The model with the best least squares regression fit was selected based on r^2 values, and for those with

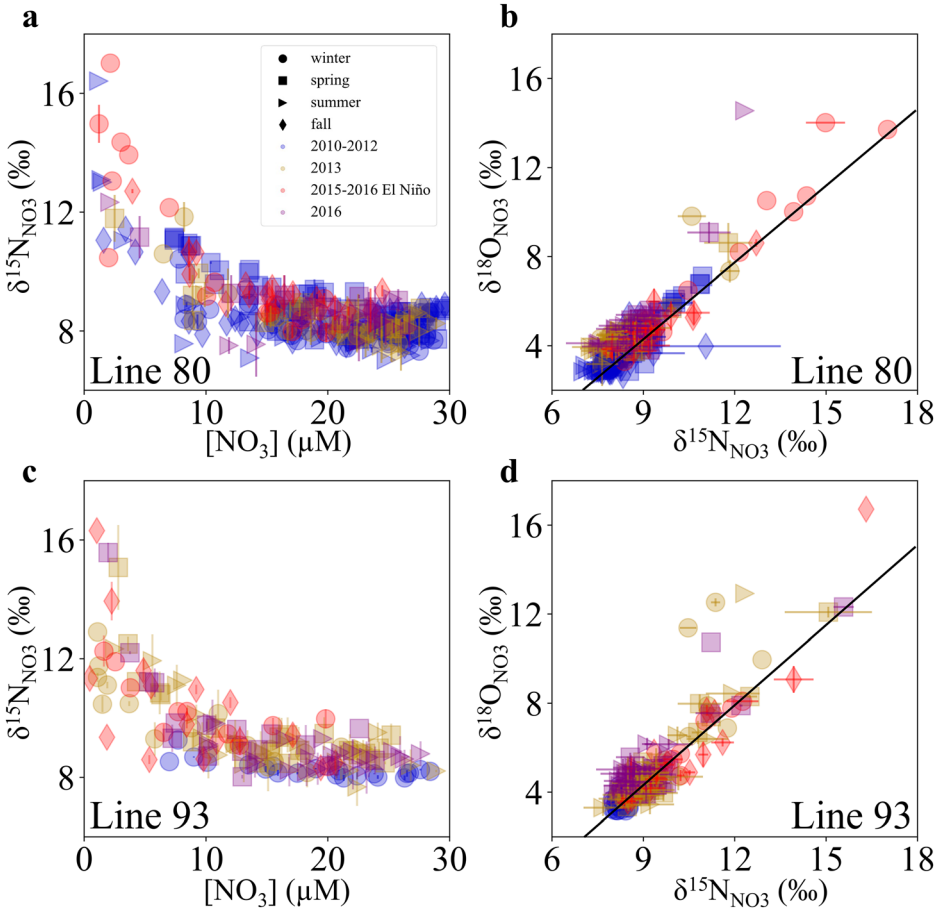

FIG. 2. $\delta^{15}N_{NO3}$ increases as NO_3^- is drawn down by phytoplankton in the surface ocean along the northern line (Line 80) (**a**) and the southern line (Line 93) (**c**). The variation in $\delta^{15}N_{NO3}$ values observed for a given NO_3^- concentration demonstrates how isotopic measurements provide additional information not available from concentration measurements alone. $\delta^{15}N_{NO3}$ and $\delta^{18}O_{NO3}$ along the northern line (**b**) and the southern line (**d**) generally increase in a ratio of 1 : 1 (indicated by the black line), but other processes such as euphotic zone nitrification can lead to deviations from this 1 : 1 trajectory. Season and year are indicated by the shape and color, respectively, of each point. Error bars show the analytical error of individual isotope measurements where they are available.

$r^2 > 0.85$, the corresponding $^{15}\varepsilon$ values are reported (Supplementary Table S2).

Estimating nitrate utilization

The nitrogen isotope data together with the appropriate Rayleigh fractionation model were used to translate measured NO_3^- isotope compositions into the fraction of upwelled NO_3^- used by phytoplankton (reported for Stas. 55–80 for Line 80 and Stas. 30–60 for Line 93). The closed system Rayleigh fractionation model was ultimately used to calculate the extent of NO_3^- utilization at each depth because more than 75% of the profiles where an isotope effect could be determined fit the closed system model better (Supplementary Table S2). Because we were unable to calculate a profile-specific isotope effect for the majority of our data, a consistent $^{15}\varepsilon$ value of 3.2 ‰ was used for all stations based on our average calculated isotope effect and isotope effects calculated from previous work conducted in the same region (Stephens et al. 2019; $^{15}\varepsilon = 3.0 \pm 0.5$ ‰). Uncertainty for the fraction of NO_3^- utilized was estimated using standard error propagation from the standard deviation of $^{15}\varepsilon$ values generated in this study (± 0.8 ‰) and the analytical error associated with our isotope measurements. The depth of the first NO_3^- use, needed to determine $\delta^{15}N_{NO3,initial}$ and the concentration of upwelling NO_3^-, was estimated from the NO_3^--temperature relationship for each station by fitting a line to NO_3^- concentration and temperature data below 150 m. The depth of the first use was assigned as the deepest depth where the measured NO_3^- value deviated below the concentration predicted from measured temperature (i.e., deviated from a simple water mass mixing relationship) by at least 2 μM, similar to the method used in Stephens et al. (2018). This method did not work for some stations, particularly during the El Niño period in 2015/2016 when surface waters were unusually warm. For stations where we were unable to use the NO_3^--temperature relationship to determine source water characteristics, NO_3^-

and Chl *a* profiles were examined individually to estimate these parameters. In this case, the NO_3^- concentration at the deepest depth where Chl *a* concentrations began to exceed background values was used (Supporting Information Fig. S1). To determine the source NO_3^- isotope composition, the closest depth below that where NO_3^- utilization had occurred was used (Supplementary Table S3). This ensured that isotope characteristics ascribed to source water were uninfluenced by biological uptake. We estimated the mixed layer depth for each profile, following de Boyer Montégut et al. (2004), as the depth where density exceeds the surface density by a threshold value, which in this case was estimated to be 0.5 kg m^{-3} to best match the regional hydrography. Results for all profiles with NO_3^- isotope measurements are shown in Supplementary Table S3.

Estimating upper ocean nitrification

Assimilation of NO_3^- by phytoplankton results in equivalent fractionation for both N and O isotopes in the remaining NO_3^- pool (Granger et al. 2004). When $\delta^{15}N_{NO3}$ and $\delta^{18}O_{NO3}$ in the euphotic zone do not change in such a predicted 1 : 1 relationship, other processes apart from assimilation must be important. The relative magnitude of this deviation can be expressed using Δ(15,18), defined by Sigman et al. (2005) as

$$\Delta(15,18) = \left[\left(\delta^{15}N_{NO3} - \delta^{15}N_{NO3,source}\right) - {}^{15}\varepsilon_p/{}^{18}\varepsilon_p\left(\delta^{18}O_{NO3} - \delta^{18}O_{NO3,source}\right)\right] \quad (3)$$

where ${}^{15}\varepsilon_p/{}^{18}\varepsilon_p$ is 1 and the source isotope values are identified as described above. Deviation from the 1 : 1 relationship in surface waters has been attributed to active euphotic zone nitrification in combination with NO_3^- uptake by phytoplankton (Granger et al. 2004; Sigman et al. 2005; Casciotti 2016). Based on previous work in the CCS region (Ward 2005; Stephens et al. 2019; Laperriere et al. 2020) we also interpreted this pattern as evidence of upper ocean nitrification and subsequent utilization of the nitrified NO_3^-. Other processes could cause NO_3^- isotope ratios to deviate and will be addressed in the discussion. The contribution of locally nitrified NO_3^- to uptake by phytoplankton was calculated after Wankel et al. (2007) using a steady-state box model, where

$$\Delta(15,18) = f_n \times \left(\varepsilon_p - f_a \times f_w \times (\varepsilon_{ntr} - \varepsilon_a)\right) - \left(\frac{\delta^{18}O_{source} - \delta^{18}O_{source} \times f_w + (\varepsilon_p \times f_n) + (\delta^{18}O_{ntr} \times f_n \times f_w)}{1 - f_w + (f_n \times f_w)}\right) + \delta^{18}O_{source} \quad (4)$$

The model identifies the f_w value (the fraction of assimilated NO_3^- contributed by nitrification within the euphotic zone) that brings the calculated Δ(15,18) closest to the measured value for each euphotic zone sample. To calculate f_w, we focused on samples with Δ(15,18) < 0 outside of measurement error—that is, samples that had a significant deviation from the expected 1 : 1 enrichment. Here, f_n is the fraction of NO_3^- remaining relative to the source NO_3^-, ε_p (identical to ${}^{15}\varepsilon$ used above) is the nitrogen isotope effect for phytoplankton uptake of NO_3^- (with a value of 3.2 ‰ used here), f_a is the fraction of NH_4^+ assimilated by phytoplankton (a value of 0.8 was used here; Ward 2005; Wankel et al. 2007), $\delta^{18}O_{ntr}$ is the $\delta^{18}O$ of NO_3^- resulting from nitrification (a value of 1 ‰ was used here; Sigman et al. 2009; Buchwald et al. 2012), and ε_a is the isotope effect of NH_4^+ assimilation (a value of 4 ‰ was used here; Sigman and Fripiat 2019). Large ranges have been reported in the literature for the combined isotope effect of nitrification (ε_{ntr}), but we note that the model is sensitive only to the difference between ε_{ntr} and ε_a, and not to their absolute values. We tested the sensitivity of the model to a range of values of ε_{ntr} and found that as ε_{ntr} decreases, the model is less effective at matching the measured values of Δ(15,18) (Supporting Information Fig. S2). Based on this analysis and on values of ε_{ntr} measured in a coastal field study (Sugimoto et al. 2009), we used an ε_{ntr} of 20 ‰ in the model. For samples where the modeled Δ(15,18) was more than 1 ‰ different from the measured Δ(15,18) indicating a poor fit to the data, resulting f_w values are not discussed further. These were mostly samples with very negative Δ(15,18) values. We note that many of the samples from 2010 to 2012 with lower NO_3^- concentrations were not analyzed for oxygen isotopes, and thus are not included in the f_w analysis.

The f_w approach is a model construct that attempts to simplify a dynamic system that alternates between steady state and "episodically driven" nutrient inputs to the upper ocean. Previous studies (Wankel et al. 2007; Stephens et al. 2019) have found that the steady-state approach adequately approximates this system, although we recognize that the model is not a perfect characterization of the true complexity of upper ocean nitrogen dynamics. Importantly, the model does allow us to place some quantitative bounds on the contribution of nitrification to nitrate uptake by phytoplankton represented by the measured Δ(15,18) values.

Calculation of stratification index

Nitrate isotopes in the upper 150 m varied spatially, seasonally, and interannually. For high values, we tested the hypothesis that more complete NO_3^- utilization linked to decreased NO_3^- supply might be responsible. Since upwelling is the major source of NO_3^- to the coastal euphotic zone of this region, decreases in NO_3^- supply may be linked to greater stratification. To examine the potential influence of stratification on N cycle parameters, we computed a stratification strength index for each station and timepoint using the density at 200 m as a reference point and calculating the difference in density between each depth in the euphotic zone and the reference density (Behrenfeld et al. 2006) (*see* Supplementary Table S4 for a complete list of density values used). To compare f_w values at high and low stratification and high and

low Chl *a* concentration, we performed a non-parametric two-sided Mann–Whitney *U*-test.

Results

Variability in stable isotopes of nitrate

Assimilation of NO_3^- by phytoplankton in the euphotic zone results in one of the strongest signals in oceanic $\delta^{15}N_{NO3}$ and $\delta^{18}O_{NO3}$ (Altabet and Francois 1994; Casciotti 2016). From 2010 to 2016, $\delta^{15}N_{NO3}$ and $\delta^{18}O_{NO3}$ above 150 m demonstrated considerable spatial and temporal variability. $\delta^{15}N_{NO3}$ ranged from 7.1 to 17.0 ‰ and $\delta^{18}O_{NO3}$ ranged from 2.7 to 16.7 ‰. Values for both $\delta^{15}N_{NO3}$ and $\delta^{18}O_{NO3}$ were highest where NO_3^- concentrations were drawn low as the result of uptake by phytoplankton. NO_3^- isotope ratios were generally higher deeper in the water column along the southern line compared to the northern line (Fig. 3), consistent with lower nitrate supply at the southern line. Upwelling source values also varied. Source $\delta^{15}N_{NO3}$ ranged from 7.4 to 9.6 ‰ along the northern line and 7.7 to 10.5 ‰ along the southern line. Source $\delta^{18}O_{NO3}$ ranged from 2.8 to 5.3 ‰ along the northern line and 3.2 to 5.6 ‰ along the southern line. Greater isotopic enrichment in source waters is expected for the southern line because this region experiences greater influence from the California Undercurrent, which flows poleward from the eastern tropical North Pacific oxygen deficient zone, where denitrification strongly fractionates nitrate isotopes (Castro et al. 2001). For the most part, both $\delta^{15}N$ and $\delta^{18}O$ increased in a ratio of 1 : 1, as would be expected for NO_3^- uptake by phytoplankton. However, some values deviated from the expected 1 : 1 relationship, and in most of these cases, $\delta^{18}O$ values were more enriched than would be predicted from the measured $\delta^{15}N$ values (Fig. 2b,d). Specifically, we identified 48 samples (19% of EZ values) where this deviation, expressed relative to the upwelling NO_3^- isotope composition as $\Delta(15,18) < 0$, was significant (*see* error discussion above), and 21 of these samples (8%) had a $\Delta(15,18)$ value < -1.

El Niño conditions, defined here as including fall 2015 to winter 2016 (Jacox et al. 2016; Lilly and Ohman 2021), resulted in large density anomalies in the surface ocean (Supporting Information Fig. S3), increased stratification (Supporting Information Figs. S4, S5), greater sea level anomalies near San Diego (Lilly and Ohman 2021; Supporting Information Fig. S6), and decreased net primary production (NPP; Supporting Information Fig. S7). At the more inshore stations, the highest $\delta^{15}N$ and $\delta^{18}O$ values were found during this time period, also coinciding with higher values deeper in the water column compared to non-El Niño conditions (Fig. 3). In the shallow surface ocean, particularly in the offshore region along the northern line and for most of the southern line, low NO_3^- concentrations prevailed and precluded isotopic measurements (Fig. 4a,c). During 2013, values of $\delta^{15}N_{NO3}$ along the southern line were almost as high as during the 2015–2016 El Niño, but fewer measurements before 2013 make it difficult to evaluate how typical these observations might be for this section of the CalCOFI grid (Fig. 4d).

Nitrate utilization

Much of the observed variability in NO_3^- isotopes likely results from incomplete NO_3^-utilization. To relate the observed isotope ratios to the variability in nitrate utilization,

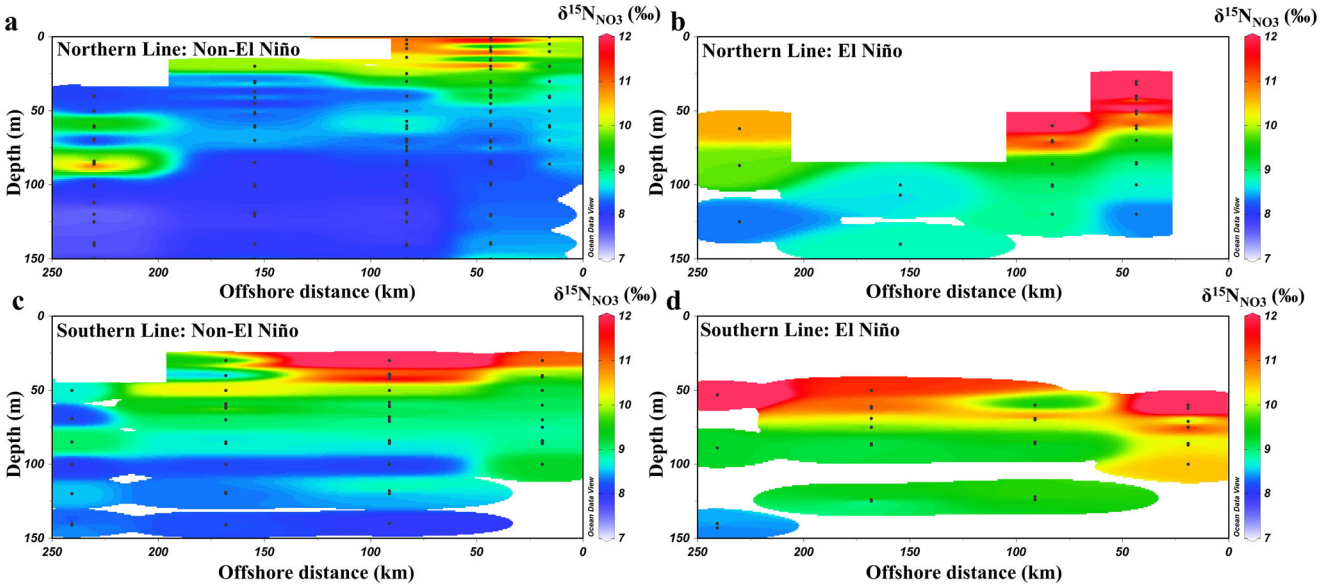

FIG. 3. Averaged $\delta^{15}N_{NO3}$ from 2010 to 2013 along the northern line is shown in (**a**), in contrast to the higher values observed during the El Niño (averaged fall 2015 to winter 2016) (**b**). A similar pattern was seen along the southern line (**c**), where $\delta^{15}N_{NO3}$ is higher deeper in the water column during the El Niño (**d**).

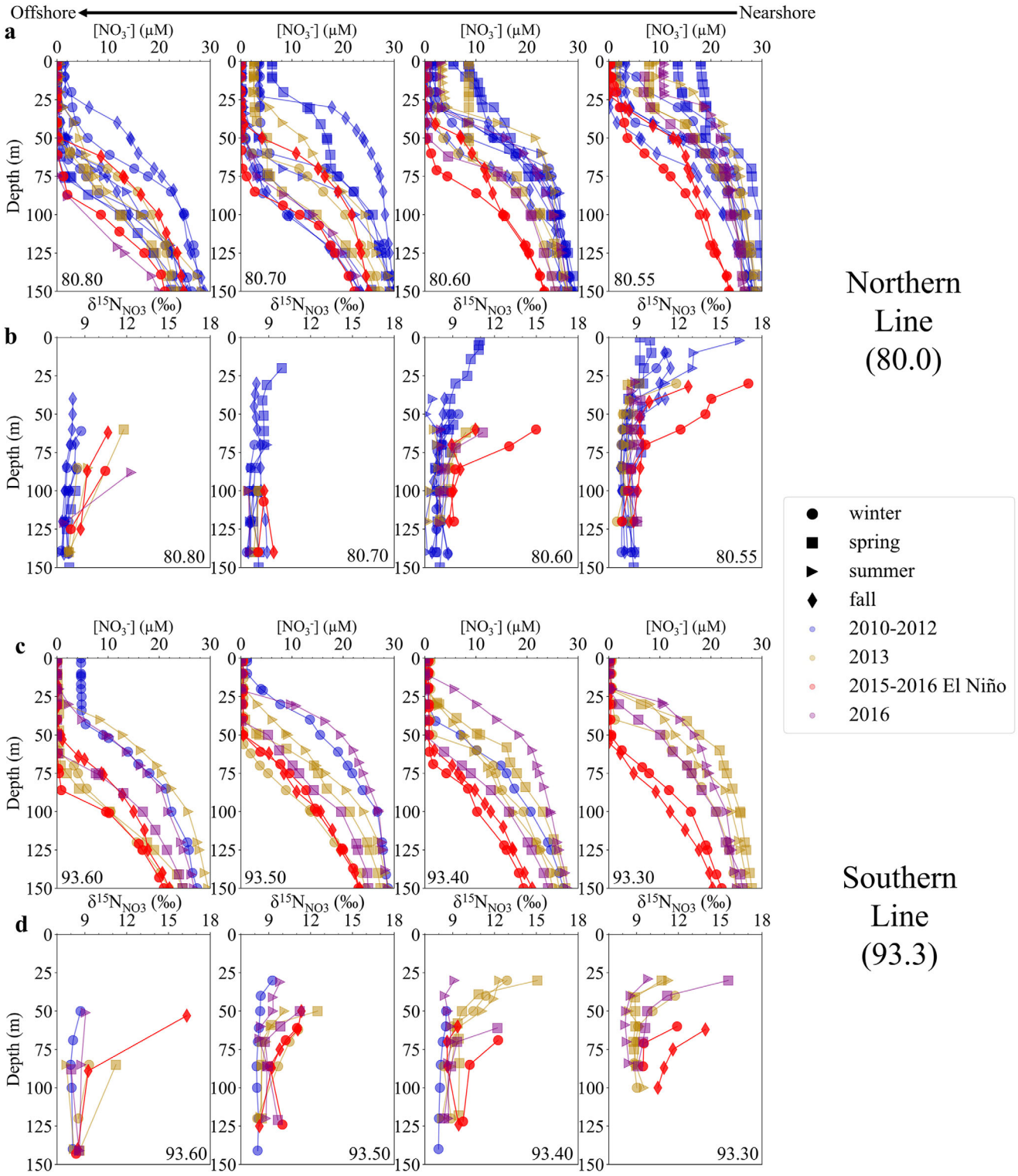

FIG. 4. NO_3^- concentrations are shown in (**a**) for the northern line and (**c**) for the southern line, with lower concentrations apparent during 2015–2016 (El Niño; red symbols). $\delta^{15}N_{NO3}$ values are plotted for all samples above 150 m in (**b**) for the northern line and (**d**) for the southern line showing larger increases during 2015–2016 compared to earlier years. Season and year are indicated by the shape and color, respectively, of each point.

an accurate estimate of the isotope effect associated with NO_3^- uptake by phytoplankton is necessary. Estimated isotope effects from the closed system profiles ranged from 2.1 to 5.0 ‰ with an average of 3.2 ± 0.8 ‰ (Supplementary Table S2). This is in good agreement with a previous study which estimated the average $^{15}\varepsilon$ for the inshore southern California Current System at 3.0 ± 0.5‰ (Stephens et al. 2019), but it is lower than what has been determined in other experimental and marine field studies (e.g., Granger et al. 2004; Casciotti 2016 and references therein).

Translation of $\delta^{15}N_{NO3}$ profiles into vertical trends in NO_3^- utilization enabled us to examine the spatial and temporal variability of this control on upper ocean $\delta^{15}N_{NO3}$ (Fig. 5). Overall, the variability observed in $\delta^{15}N_{NO3}$ values was primarily driven by large changes in the fraction of NO_3^- utilized, which varied from zero up to 0.94 at specific depths. Along the northern line, $\delta^{15}N_{NO3}$ values were driven primarily by incomplete utilization during spring cruises (Fig. 5). Apart from 2016, the fraction of NO_3^- utilized did not rise above 0.50 for spring cruises, and surface NO_3^- concentrations remained elevated at inshore stations (Fig. 4a). For most other seasons, very few $\delta^{15}N_{NO3}$ values were recorded near the surface due to near complete utilization of NO_3^-. Below the surface, the shape of the NO_3^- utilization profile often differed significantly between seasons. Of the winter cruises, January 2016 (the winter of El Niño) saw the greatest fraction of NO_3^- utilization (reaching above 0.5 at 60–75 m for both Stas. 80.55 and 80.60) whereas for all summer cruises, the fraction of NO_3^- utilized remained below 0.5 at depths where we had $\delta^{15}N_{NO3}$ measurements (> 20 m). The influence of El Niño was noticeable in $\delta^{15}N_{NO3}$ values during the November 2015 cruise, and during this time, we observed enriched values associated with more complete NO_3^- utilization at every depth compared to previous fall datasets. Limited sampling of the southern line makes it more difficult to consider seasonal differences. The most robust trend was the rapid increase in $\delta^{15}N_{NO3}$ at deeper depths associated with strong depth gradients in NO_3^- utilization during the 2015–2016 El Niño.

Iron limitation estimated from silica excess

Given that the extent of NO_3^- utilization strongly impacts $\delta^{15}N_{NO3}$, we examined potential controls on NO_3^- utilization. Iron limitation of phytoplankton productivity has been shown to occur intermittently in this region (King and Barbeau 2007; Hogle et al. 2018; Stukel and Barbeau 2020) and could be responsible for limiting NO_3^- utilization. Excess

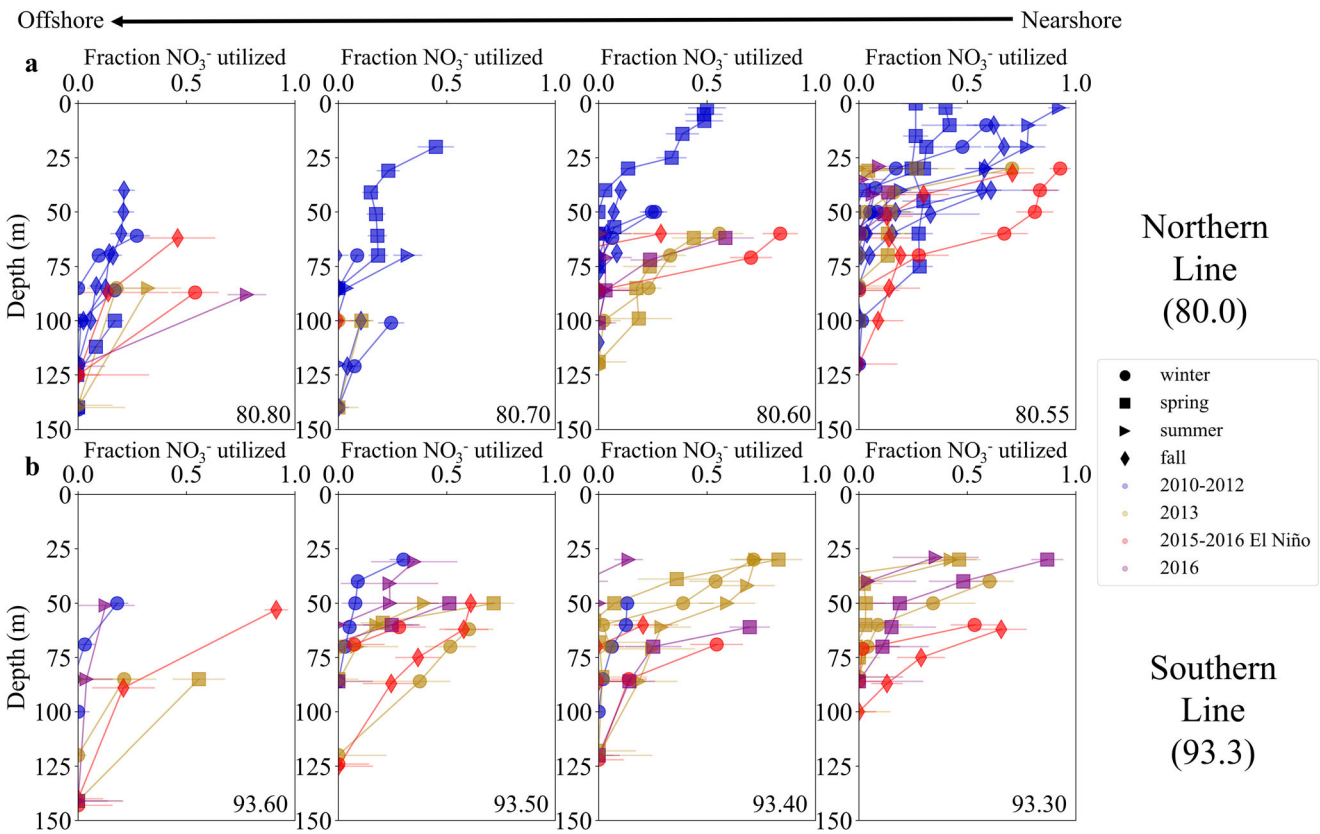

FIG. 5. The fraction of NO_3^- that was utilized at individual depths in shown for the northern line (Line 80) (**a**) and southern line (Line 93) (**b**). Error bars were calculated based on analytical errors of isotope measurements and standard deviation of estimated $^{15}\varepsilon$. Season and year are indicated by the shape and color, respectively, of each point.

silica relative to nitrate, Si_{ex}, where $Si_{ex} = [Si(OH)_4] - (R_{Si:NO3} \times [NO_3^-])$, has been previously used as an indicator of possible iron limitation in the CCS (Hogle et al. 2018; Stukel and Barbeau 2020). Negative values of Si_{ex} are thought to result from Fe-limited diatoms taking up excess silicic acid ($Si(OH)_4$) relative to NO_3^- compared to $R_{Si:NO3}$ in upwelling waters (Hutchins and Bruland 1998). For this calculation, $R_{Si:NO3}$ was determined in the same way as upwelling NO_3^- isotope ratios (as described above). Profiles of Si_{ex} for the northern line and the southern line are shown for each station in Fig. 6. Si_{ex} invariably becomes positive in the surface ocean when all the NO_3^- has been consumed (Figs. 4a,c, 6). Positive values show that excess silica accumulates at these depths (relative to upwelling values) and are indicative of NO_3^- uptake by phytoplankton with lower or no silica requirements. This trend is reflected in size-fractionated Chl *a* data (Supporting Information Figs. S8, S9). For example, the picophytoplankton (< 1 μm) community, which is not expected to be dominated by diatoms, was prominent at Sta. 80.55 during January 2013 and 2016 (Supporting Information Fig. S7), and values in the corresponding Si_{ex} profile are ≥ 0 (Fig. 6a). This contrasts with January 2011, when Chl *a* was primarily present in larger cell sizes (> 3 μm) at Sta. 80.55, likely dominated by diatoms, and Si_{ex} values are ≤ 0.

Along the northern line, Si_{ex} is often more negative in the upper ocean further offshore, developing primarily in the spring and summer, but also occasionally in the fall. For the southern line, it is the inshore stations that display the strongest (deep) Si_{ex} minimum, which develops primarily during the spring and summer (Fig. 6: e.g., Sta. 93.30) and appears at depths ≥ 40 m.

Euphotic zone nitrification

For samples above 100 m, Δ(15,18) ranged from −5.9 to 1.6 ‰ (Supporting Information Fig. S10). Negative values signify that either the $\delta^{15}N_{NO3}$ is anomalously low, or that the $\delta^{18}O_{NO3}$ is anomalously elevated relative to what would be expected based on source NO_3^- isotope values enriched only via the process of NO_3^- assimilation (Wankel et al. 2007; Casciotti 2016). Negative Δ(15,18) values could also result from low $\delta^{15}N_{NO3}$ derived from N_2 fixation and atmospheric deposition of nitrogen (Altieri et al. 2021) and their potential influence will be discussed later. Here, we assume that negative deviations are due to the presence of NO_3^- produced via

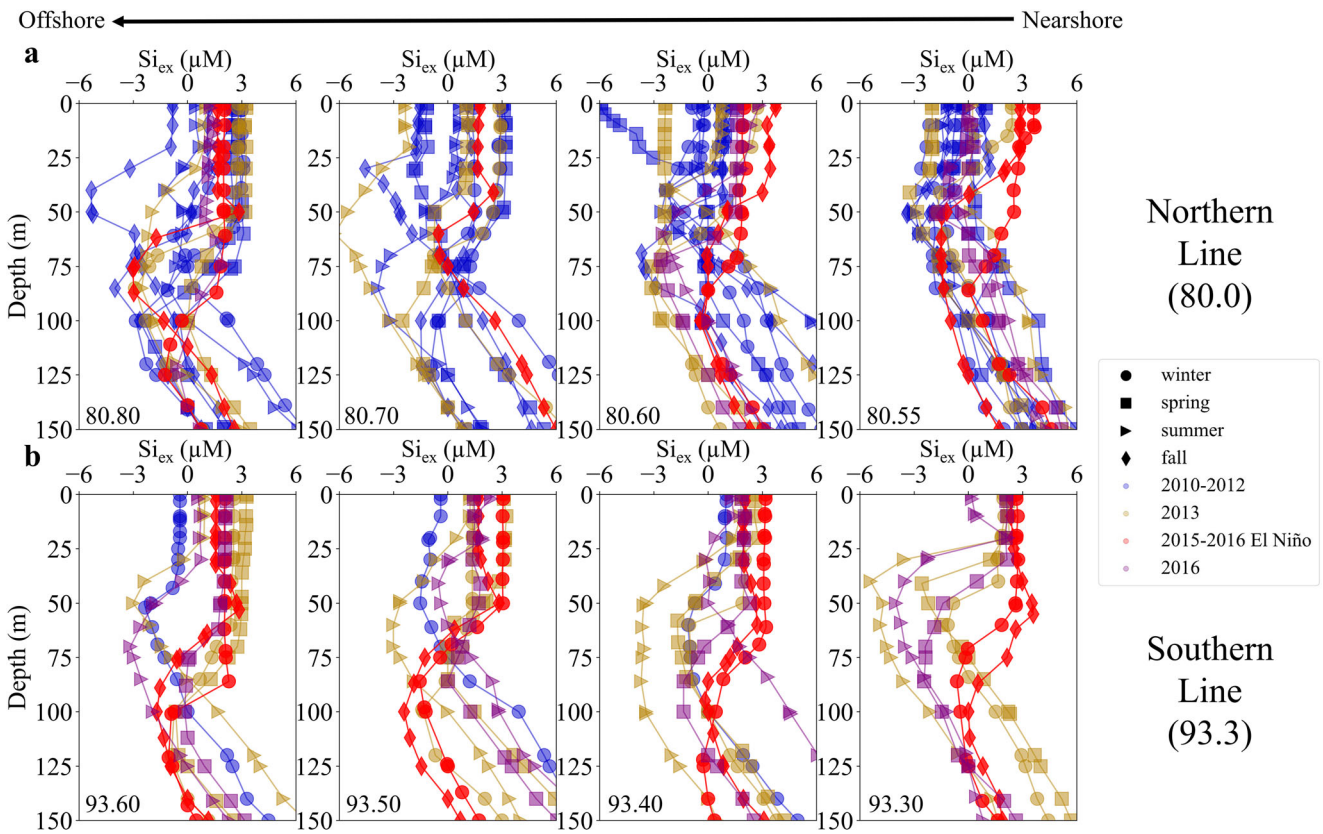

FIG. 6. Profiles of Si_{ex} are shown here for the northern line (Line 80) (**a**) and southern line (Line 93) (**b**) for each station. Season and year are indicated by the shape and color, respectively, of each point. Along the northern line, values become more negative moving offshore. Along the southern line, the more inshore stations exhibit strong mid-depth minima in Si_{ex}. We note that for each profile Si_{ex} is, by definition, zero at its upwelling depth.

local (euphotic zone) nitrification, which has the effect of elevating $\delta^{18}O_{NO3}$ but not $\delta^{15}N_{NO3}$, relative to assimilation alone. The fractional contribution of nitrification to NO_3^- uptake by phytoplankton (f_w) varied spatially and temporally, ranging from 0 to more than 0.9 at individual depths (Fig. 7a,b).

Increased contribution from euphotic zone nitrification occurred when ocean waters were warmer and more stratified (per the stratification strength index) and NO_3^- concentrations in the euphotic zone were lower (Figs. 4, 7c). Comparing samples from highly stratified (> 1.1) and less stratified (< 1.1) waters revealed a highly significant difference in f_w (Mann–Whitney *U*-test; $p < 0.0001$). Samples with higher Chl *a* concentrations ([Chl *a*] > 1.8 μg L^{-1}) also had significantly lower f_w (Mann–Whitney *U*-test; $p < 0.01$; Fig. 7d), although the difference was less pronounced than for the stratification index. It is difficult to estimate an average f_w value due to variations in spatial sampling, but in general, the contribution from nitrification was low for most time periods. Out of 206 calculated f_w values, only 21 were above 0.2. These elevated values appeared mainly along the southern line (Fig. 7b; 17 out of 96 measurements from Line 93 had f_w above 0.2) and during winter 2016 for the northern line (Fig. 7a; two out of six measurements from Line 80 during winter 2016 had f_w above 0.2). Because the majority of data points on the southern line are from 2013 and 2015–2016, when the upper ocean was warm and stratified, we cannot determine whether Line 93 would regularly exhibit high f_w. In fact, a time series of satellite-based NPP estimates for inshore stations shows an extended period of low NPP along the southern line from 2013 to mid-2016 (Supporting Information Fig. S7) indicating that this time period was anomalous and may have indeed seen decreased NO_3^- input from vertical transport. Such episodes could favor NPP supported primarily by recycled nutrients, including NO_3^- derived from euphotic zone nitrification. All elevated f_w values occurred within a relatively narrow depth range of 30–70 m (Fig. 7a,b).

As noted above, we observed relatively low values for $^{15}\varepsilon$, and low $^{15}\varepsilon$ values have previously been attributed to the

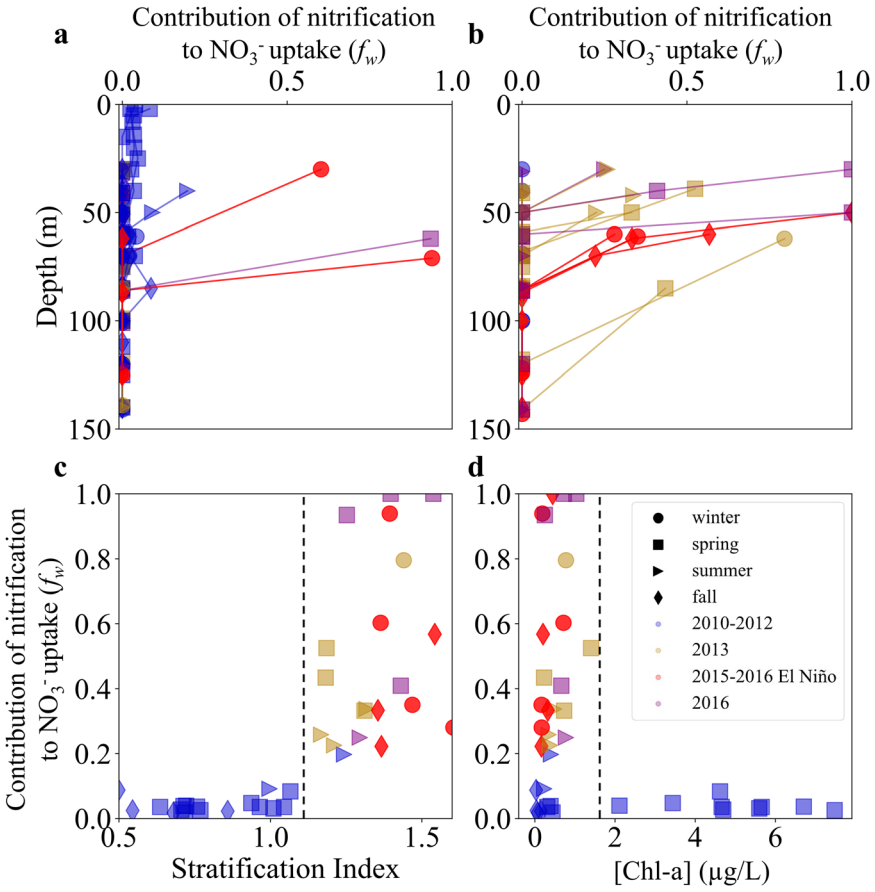

FIG. 7. The proportion of NO_3^- taken up by phytoplankton that originated from nitrification in the euphotic zone (f_w) by depth (northern line, (**a**); southern line, (**b**)) and as compared to the stratification strength index (**c**) and Chl *a* concentration (**d**). f_w was greater during warm periods when the water column was more stratified, and upwelling was reduced. Higher f_w values were also associated with lower concentrations of Chl *a* for similar depths. Season and year are indicated by the shape and color, respectively, of each point. The black dotted lines indicate the two groups compared using a Mann–Whitney test.

influence of nitrification (Smart et al. 2015). This is a possible explanation for our observations, as lower $^{15}\varepsilon$ and higher f_w both corresponded to lower NPP in our dataset (Supporting Information Fig. S11; Pearson $r = 0.408$, $p = 0.116$). However, we were unable to identify a relationship between $^{15}\varepsilon$ and higher f_w, and some profiles with $^{15}\varepsilon \sim 3$ ‰ showed no evidence that nitrification was important (Supplementary Table S2).

Discussion

This study examined the climatology, hydrography, and biology that influence NO_3^- isotopes in the southern California Current System, a productive marine environment with significant ecological and economic value. Motivated by the need to prepare for the future, there is widespread interest in understanding why productivity in the region has varied in the past. As a result, a variety of nitrogen isotope archives, including sediments and preserved biological specimens, have been used to examine past variations in the NO_3^- supply to the euphotic zone. However, direct measurements of NO_3^- isotopes are limited. This study presents the largest dataset of NO_3^- isotopes from the eastern North Pacific Ocean and is thus able to provide insight into seasonal, interannual, and spatial variations that are linked to natural climate variability, micronutrient limitation, and N transformation processes in the euphotic zone.

Influence of ENSO on nitrogen cycling

We observed differences between $\delta^{15}N_{NO3}$ measured during El Niño and non-El Niño periods both in the magnitude of the values (Figs. 2–4) as well as in the NO_3^- dynamics inferred from isotope ratios (Figs. 5, 7, 8). More complete NO_3^- utilization by upper ocean ecosystems during this period resulted in elevated $\delta^{15}N_{NO3}$ values, with strong vertical gradients visible deeper in the water column during El Niño (Fig. 5). These signatures pointed to an overall decrease in NO_3^- supply to the euphotic zone consistent with a deeper nitracline and reduced upwelling (Jacox et al. 2016; Bograd et al. 2019). Estimates of greater utilization confirm that the observed enrichment in N isotopes during previous El Niño events could be explained by decreased supply and does not require elevated $\delta^{15}N$ values in source nitrate, as had been previously hypothesized (Rau et al. 2003).

The larger fraction of NO_3^- assimilated by phytoplankton that was derived from recycled nitrogen (Fig. 7a,b), particularly along the southern line, also reflects the importance of euphotic zone nitrification during the 2015–2016 El Niño. The temporal variability of this dataset suggests that the decreased supply of NO_3^- from below moves the CCS toward an increased reliance on NO_3^- derived from nitrification. Our data cannot determine whether the nitrification rate itself increased during this time. However, the decreased vertical mixing and deeper pycnocline (Supporting Information Fig. S3) could have resulted in longer residence times of suspended particulate organic nitrogen in the euphotic zone, which could have supplied additional NH_4^+ upon remineralization and led to increased nitrification rates during this El Niño event. Overall, the increased relative contribution from recycled nitrogen reported here is consistent with previous studies from the region that have reported decreased new production—primary production supported by nitrate upwelled from below—during El Niño years (Hernández-de-la-Torre et al. 2003; Kelly et al. 2018).

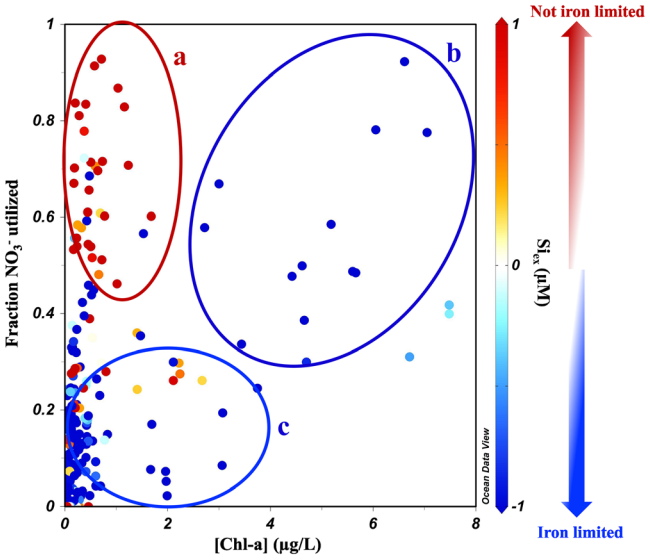

FIG. 8. A comparison of [Chl *a*], the fraction of NO_3^- utilized, and the proxy for diatom iron limitation Si_{ex} (color bar). The range of Si_{ex} values is greater than −1 to 1 (Fig. 6) but was shortened here to simplify interpretation. Negative values of Si_{ex} indicate potential iron limitation (blue). Three different groups of data points, identifying different ecosystem conditions (iron replete: (**a**), and iron limited: (**b**, **c**)), were identified and discussed further in the text.

Warming increases importance of local nitrification

Elevated reliance on nitrified NO_3^- by phytoplankton has been previously reported in this region, and generally occurred at times of low NPP (Figs. 7d, S1, S7), indicating the importance of recycled NO_3^- in maintaining food webs during these periods (Peng et al. 2018; Stephens et al. 2019; Laperriere et al. 2020). As noted in previous studies (e.g., Ward et al. 1989; Dore and Karl 1996; Smart et al. 2015), new production estimates that rely on NO_3^- uptake measurements would be impacted if a significant fraction of NO_3^- in the euphotic zone were derived from nitrified NO_3^- (Yool et al. 2007). In addition to the El Niño, we also observed elevated f_w along the southern line in 2013 during non-El Niño periods (Fig. 7b). Our data showed increased f_w and NO_3^- utilization in 2013 and 2015–2016, so it is likely that the warm anomaly years between 2013 and 2015 exhibited similar conditions (e.g., Stephens et al. 2019) particularly along the

southern line. Across our entire dataset, we observed that f_w is higher when the water column is more stratified (Fig. 7c), and when the stratification index was > 1.4 in our dataset more than half of the NO_3^- used by phytoplankton came from the euphotic zone nitrification. This does not mean that nitrification rates increased during these more stratified periods, only that the relative importance of nitrified nitrate to NPP was greater.

All f_w values above 0.25 occurred when Si_{ex}, our proxy for iron limitation, was positive (i.e., no evidence of iron limitation). This could be explained by an oligotrophic phytoplankton community dominated by non-diatom phytoplankton, consistent with the observed trends in size-fractionated chlorophyll (Supporting Information Figs. S8, S9). The CalCOFI time series of flow cytometry-based phytoplankton community composition (Nagarkar et al. 2021) also indicated that warm periods, when we expect greater f_w values, are correlated with a phytoplankton community of smaller cells including autotrophic cyanobacteria. Another recent study observed lower biogenic silica to Chl *a* ratios during the period of the warm anomaly, suggesting a decrease in the abundance of siliceous phytoplankton at that time (Closset et al. 2021). Taken together, positive Si_{ex} values coincident with higher f_w do not mean that iron limitation was unimportant, rather it could mean that the influence of iron limitation was not recorded by Si_{ex} due to the absence of diatoms. Limited evidence suggests that some nitrifiers can experience iron limitation in the surface ocean, and thus may not be as active when they are having to compete with phytoplankton for scarce iron (Shafiee et al. 2019). This could be another reason why f_w values appear elevated only when we do not see indicators of iron limitation.

As we do not have measurements of NO_3^- or NH_4^+ uptake from CalCOFI cruises, we are unable to comment either on how nitrification rates or NH_4^+ uptake rates varied here, or to link these rates to f_w. It is also unclear how f_w is related to the f-ratio (the ratio of new to total production), as it has been suggested that phytoplankton and nitrifiers compete for access to NH_4^+ (Ward and Carlucci 1985; Ward 2005; Smith et al. 2014). There is a tendency for the f-ratio to decrease alongside NPP, and so, lower fluxes of vertically supplied NO_3^- have important ramifications for higher trophic level productivity and carbon export (Eppley et al. 1977). It is possible that higher temperatures resulted in higher organic matter recycling rates and therefore, higher nitrification rates as well (Wohlers et al. 2009). These questions could be addressed in future studies that are able to consider nitrification and NH_4^+ uptake by phytoplankton together. Additional isotope studies would also benefit from the collection of higher resolution profiles, where a robust integrated f_w could be calculated.

Our focus on f_w, and thus euphotic zone nitrification, assumes that anomalously high $\delta^{18}O_{NO3}$ leads to the negative Δ(15,18) values observed in our dataset. However, negative Δ(15,18) values could also result from anomalously low $\delta^{15}N_{NO3}$ values, supplied, for example, from N derived from N_2 fixation or atmospheric N deposition (Altieri et al. 2021). N_2 fixation rates have been reported for this region (Mills et al. 2020). Just south of the CalCOFI domain, N_2 fixation was shown to account for 4%–5% of total production and between 8% and 83% of new production (Turk-Kubo et al. 2021). As such, we cannot discount this potential influence on $\delta^{15}N_{NO3}$. Atmospheric deposition on the other hand may be most relevant for surface waters and unlikely to influence the deeper f_w values determined in this study. Future studies should examine the potential role of N_2 fixation on Δ (15,18), particularly during times of pronounced upper ocean stratification. Here, we chose to interpret negative Δ(15,18) values in the context of nitrification because upper ocean nitrification is a well-established phenomenon in the region (e.g., Ward 2005; Wankel et al. 2007; Santoro et al. 2010).

Incomplete nitrate utilization

Recent studies have indicated that both Ekman transport associated with coastal upwelling as well as iron limitation in the California Current can limit NO_3^- utilization in nearshore waters, allowing excess NO_3^- and nitrogen biomass to be transported offshore or subducted at fronts (Plattner 2005; Frischknecht et al. 2018; Hogle et al. 2018). Capturing these events of incomplete NO_3^- utilization is also important for interpreting isotope studies of non-nitrate N reservoirs. In our dataset, inshore stations along the northern line off Point Conception likely experienced lower fractions of NO_3^- utilization due to the rapid transport of upwelling waters offshore (Fig. 5). For example, some profiles of NO_3^- isotopes exhibit open system dynamics where marked isotope fractionation is not discernible from depth profiles (Fig. 4b, e.g., at 80.55). Although there is little isotopic enrichment, it is clear from profiles of [Chl *a*] that significant primary production is occurring at these stations (Fig. S1a).

Inshore, upwelling conditions lead to nutrient-replete surface waters necessary to support diatom blooms. With their higher iron quotas and requirements for silica, diatoms will influence the Si : NO_3^- ratio, and thus Si_{ex} (King and Barbeau 2007; Brzezinski et al. 2015). Negative values of Si_{ex} indicate that diatoms are using more Si relative to NO_3^-, as is the case with iron-limited diatoms (Hutchins and Bruland 1998). Light limitation can also result in preferential consumption of Si relative to NO_3^-, but previous work by Hogle et al. (2018) showed that inshore along the southern line, Fe limitation rather than co-limitation (i.e., Fe and light) was the dominant control on diatom production. Our dataset suggests that NO_3^- utilization and Si_{ex} interact in a few different ways.

First, water masses with positive Si_{ex} values but low Chl *a* (Fig. 8a) are likely nitrate-limited and more oligotrophic. In these environments, NO_3^- has been drawn down, but the overall limited supply of NO_3^- keeps Chl *a* concentrations low. We can see from the size-fractionated chlorophyll data

that these communities tend to host smaller phytoplankton, potentially with either no or limited silica requirements (Supporting Information Figs. S8, S9). Although it is possible that these communities are also experiencing iron limitation, it will not be reflected in the Si_{ex} proxy used here. However, iron limitation of both phytoplankton and heterotrophic bacteria has been shown to be less common in oligotrophic regimes (Kirchman et al. 2000). It is also possible that the same conditions which may favor recycling of nitrogen also result in greater iron recycling, potentially alleviating iron limitation (Rafter et al. 2017). These conditions generally describe what was commonly observed during the 2015–2016 El Niño (Figs. 3, 4a,c).

Any unutilized iron supplied from sediments or from external sources is oxidized or scavenged quickly unless chelated by iron-binding ligands (Gledhill and Buck 2012), and coastal diatoms have been shown to concentrate iron for long-term storage under iron-replete conditions (Lampe et al. 2018). For these reasons, upwelling water masses can rapidly tend toward iron limitation as they move offshore. Indeed this has been previously demonstrated specifically for Point Conception (Firme et al. 2003; King et al. 2012). In regions with high NO_3^- utilization and high [Chl *a*], we propose that developing iron limitation in offshore moving water masses may be responsible for the negative Si_{ex} values (Fig. 8b) at Stas. 80.60, 80.70, and 80.80 (Fig. 6a). Iron limitation offshore along the northern line has been identified in other studies (e.g., Brzezinski et al. 2015).

Finally, negative Si_{ex} values indicative of iron limitation were found to coincide with lower Chl *a* and lower NO_3^- utilization (as indicated by $\delta^{15}N_{NO3}$) inshore along the southern line (Fig. 8c). At these locations, negative Si_{ex} values appeared deeper in the water column and under more stratified conditions (Figs. 6, S4). Subsurface, negative Si_{ex} values are consistent with previous studies that have identified subsurface Chl *a* maxima as important sites of iron limitation along the southern line (Hogle et al. 2018). At these depths, diatoms experiencing light limitation may produce a greater number of photosystems (Strzepek et al. 2019), resulting in even greater iron requirements. Long-term records of CalCOFI Si_{ex} suggest that diatoms are becoming increasingly iron limited, consistent with a secular surface ocean warming trend and increased stratification leading to the development of iron limitation at the base of the euphotic zone (Hogle et al. 2018). It is possible that this will result in a reapportionment of nutrients, and thus productivity, in the region, as unutilized NO_3^- may become available for export elsewhere.

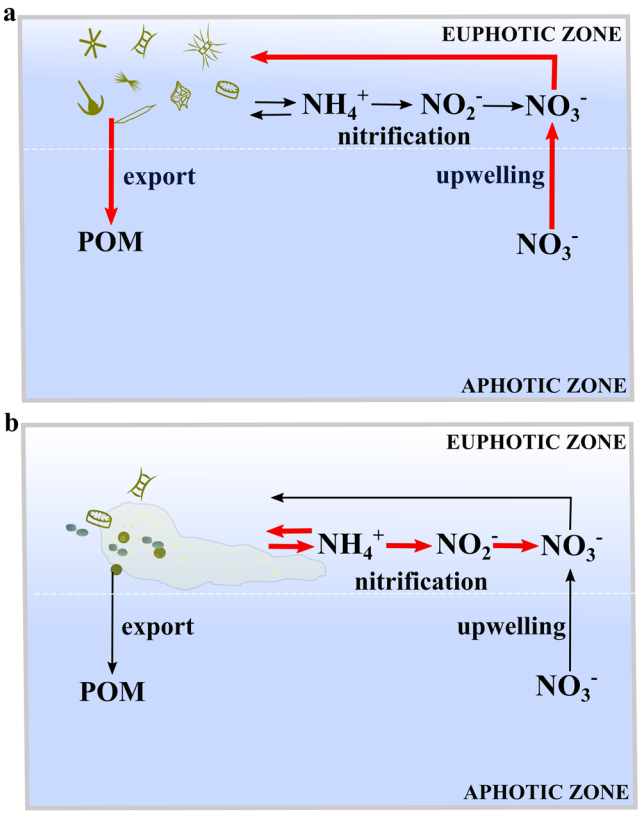

FIG. 9. El Niño alters N cycling. During average conditions (**a**), NO_3^- is supplied via upwelling which fuels high productivity and the growth of larger phytoplankton such as diatoms, which in turn leads to high export fluxes. Although nitrification is taking place in the euphotic zone, it is not a prominent source of the nitrate utilized by phytoplankton. During the 2015–2016, El Niño event (**b**), surface warming resulted in increased stratification, decreased nitrate supply from upwelling, and lower NPP. Phytoplankton communities were smaller, found deeper in the water column, and relied more on nitrate recycled via upper ocean nitrification. Ammonia supply for nitrification may have been enhanced by the remineralization of non-sinking detrital organic matter sources that are trapped in the euphotic zone due to stratification and a decrease in sinking export.

Conclusions

The NO_3^- isotope data presented here shed light on the N cycle impacts of the 2015–2016 El Niño in the southern California Current System (Fig. 9) and provide important context for interpreting isotope ratios preserved in N archives. Whether the response we observed in NO_3^- biogeochemistry is typical of other El Niño events remains to be seen, especially because this particular event occurred during a pronounced marine heatwave: the North Pacific warm anomaly of 2014–2015 (Di Lorenzo and Mantua 2016; Jacox et al. 2016). The El Niño conditions of late 2015 and early 2016 resulted in reduced NO_3^- supply, leading to elevated NO_3^- isotopic compositions due to more complete NO_3^- utilization. This period of warm surface waters also resulted in greater stratification, which increased the relative reliance of the phytoplankton community on NO_3^- recycled in the upper ocean (Fig. 9). Our larger dataset also revealed significant variability in upper ocean NO_3^- isotopic composition tied to differences in the extent of euphotic zone NO_3^- utilization. The degree of NO_3^- utilization and therefore nitrogen isotope fractionation is

likely influenced by iron limitation at southern, inshore stations and within the California Current along the northern line. Some inshore stations along the northern line also showed low NO_3^- utilization that was not tied to iron limitation but was likely driven by rapid Ekman transport of unused NO_3^- offshore and replacement with newly upwelled NO_3^-. Iron limitation of diatom productivity was not observed during the two cruises that sampled the region during the 2015–2016 El Niño event, likely due to the overall decrease in the abundance of large phytoplankton during this period. The dominance of smaller phytoplankton suggests that the increased NO_3^- utilization recorded by elevated nitrogen isotopes during El Niño events, especially those preceded by warm ocean conditions resembling the North Pacific Warm Anomaly, are also accompanied by increased food chain length, an ecosystem parameter that can be discerned from some N archives (Décima et al. 2013). These trends may be expected to become increasingly relevant as surface oceans continue to warm due to anthropogenic climate change.

Data availability statement

All data produced by the CalCOFI program are available at http://calcofi.org. Nitrate isotope data can be found at https://oceaninformatics.ucsd.edu/datazoo/catalogs/ccelter/datasets/284. Upwelling velocities and other model data are available at http://www.ecco.ucsd.edu/case.html.

References

Aksnes, D. L., and M. D. Ohman. 2009. Multi-decadal shoaling of the euphotic zone in the southern sector of the California current system. Limnol. Oceanogr. **54**: 1272–1281. doi:10.4319/lo.2009.54.4.1272

Altabet, M. A. 1988. Variations in nitrogen isotopic composition between sinking and suspended particles: Implications for nitrogen cycling and particle transformation in the open ocean. Deep-Sea Res. Part A. Oceanogr. Res. Pap **35**: 535–554. doi:10.1016/0198-0149(88)90130-6

Altabet, M. A., and R. Francois. 1994. Sedimentary nitrogen isotopic ratio as a recorder for surface ocean nitrate utilization. Global Biogeochem. Cycles **8**: 103–116. doi:10.1029/93GB03396

Altieri, K. E., S. E. Fawcett, and M. G. Hastings. 2021. Reactive nitrogen cycling in the atmosphere and ocean. Annu. Rev. **49**: 523–550. doi:10.1146/ANNUREV-EARTH-083120-052147

Behrenfeld, M. J., and others. 2006. Climate-driven trends in contemporary ocean productivity. Nature **444**: 752–755. doi:10.1038/nature05317

Bograd, S. J., and others. 2015. Changes in source waters to the Southern California Bight. Deep-Sea Res. Part II Top. Stud. Oceanogr. **112**: 42–52. doi:10.1016/j.dsr2.2014.04.009

Bograd, S. J., I. D. Schroeder, and M. G. Jacox. 2019. A water mass history of the Southern California current system. Geophys. Res. Lett. **46**: 6690–6698. doi:10.1029/2019GL082685

Böhlke, J. K., S. J. Mroczkowski, and T. B. Coplen. 2003. Oxygen isotopes in nitrate: New reference materials for ^{18}O: ^{17}O: ^{16}O measurements and observations on nitrate-water equilibration. Rapid Commun. Mass Spectrom. **17**: 1835–1846. doi:10.1002/rcm.1123

Brand, W. A., and others. 2009. Comprehensive inter-laboratory calibration of reference materials for δ18O versus VSMOW using various on-line high-temperature conversion techniques. Rapid Commun. Mass Spectrom. **23**: 999–1019. doi:10.1002/rcm.3958

Brzezinski, M. A., J. W. Krause, R. M. Bundy, K. A. Barbeau, P. Franks, R. Goericke, M. R. Landry, and M. R. Stukel. 2015. Enhanced silica ballasting from iron stress sustains carbon export in a frontal zone within the California current. J. Geophys. Res. Ocean. **120**: 4654–4669. doi:10.1002/2015JC010829

Buchwald, C., A. E. Santoro, M. R. McIlvin, and K. L. Casciotti. 2012. Oxygen isotopic composition of nitrate and nitrite produced by nitrifying cocultures and natural marine assemblages. Limnol. Oceanogr. **57**: 1361–1375. doi:10.4319/LO.2012.57.5.1361

Casciotti, K. L. 2016. Nitrogen and oxygen isotopic studies of the marine nitrogen cycle. Ann. Rev. Mar. Sci. **8**: 379–407. doi:10.1146/annurev-marine-010213-135052

Casciotti, K. L., D. M. Sigman, M. G. Hastings, J. K. Böhlke, and A. Hilkert. 2002. Measurement of the oxygen isotopic composition of nitrate in seawater and freshwater using the denitrifier method. Anal. Chem. **74**: 4905–4912. doi:10.1021/ac020113w

Castro, C. G., F. P. Chavez, and C. A. Collins. 2001. Role of the California undercurrent in the export of denitrified waters from the eastern tropical North Pacific. Global Biogeochem. Cycles **15**: 819–830. doi:10.1029/2000GB001324

Chan, F., J. A. Barth, J. Lubchenco, A. Kirincich, H. Weeks, W. T. Peterson, and B. A. Menge. 2008. Emergence of anoxia in the California current large marine ecosystem. Science **319**: 920. doi:10.1126/science.1149016

Closset, I., H. M. McNair, M. A. Brzezinski, J. W. Krause, K. Thamatrakoln, and J. L. Jones. 2021. Diatom response to alterations in upwelling and nutrient dynamics associated with climate forcing in the California current system. Limnol. Oceanogr **4**: 1578–1593. doi:10.1002/lno.11705

Davis, C. V., J. F. Ontiveros-Cuadras, C. Benitez-Nelson, A. Schmittner, E. J. Tappa, E. Osborne, and R. C. Thunell. 2019. Ongoing increase in eastern tropical North Pacific denitrification as interpreted through the Santa Barbara Basin sedimentary δ15N record. Paleoceanogr. Paleoclimatol. **34**: 1554–1567. doi:10.1029/2019PA003578

de Boyer Montégut, C., G. Madec, A. S. Fischer, A. Lazar, and D. Iudicone. 2004. Mixed layer depth over the global

ocean: An examination of profile data and a profile-based climatology. J. Geophys. Res. C Ocean. **109**: 1–20. doi:10.1029/2004JC002378

Décima, M., M. R. Landry, and B. N. Popp. 2013. Environmental perturbation effects on baseline δ^{15}N values and zooplankton trophic flexibility in the southern California current ecosystem. Limnol. Oceanogr. **58**: 624–634. doi:10.4319/lo.2013.58.2.0624

Di Lorenzo, E., and N. Mantua. 2016. Multi-year persistence of the 2014/15 North Pacific marine heatwave. Nat. Clim. Change **6**: 1042–1047. doi:10.1038/nclimate3082

Dore, J. E., and D. M. Karl. 1996. Nitrification in the euphotic zone as a source for nitrite, nitrate, and nitrous oxide at station ALOHA. Limnol. Oceanogr. **41**: 1619–1628. doi:10.4319/lo.1996.41.8.1619

Eppley, R. W., J. H. Sharp, E. H. Renger, M. J. Perry, and W. G. Harrison. 1977. Nitrogen assimilation by phytoplankton and other microorganisms in the surface waters of the central North Pacific Ocean. Mar. Biol. **39**: 111–120. doi:10.1007/BF00386996

Eppley, R. W., and B. J. Peterson. 1979. Particulate organic matter flux and planktonic new production in the deep ocean. Nature **282**: 677–680. doi:10.1038/282677a0

Firme, G. F., E. L. Rue, D. A. Weeks, K. W. Bruland, and D. A. Hutchins. 2003. Spatial and temporal variability in phytoplankton iron limitation along the California coast and consequences for Si, N, and C biogeochemistry. Global Biogeochem. Cycles **17**: 1016. doi:10.1029/2001GB001824

Frischknecht, M., M. Münnich, and N. Gruber. 2015. Remote versus local influence of ENSO on the California current system. J. Geophys. Res. Ocean. **120**: 1353–1374. doi:10.1002/2014JC010531

Frischknecht, M., M. Münnich, and N. Gruber. 2018. Origin, transformation, and fate: The three-dimensional biological pump in the California current system. J. Geophys. Res. Ocean. **123**: 7939–7962. doi:10.1029/2018JC013934

Gledhill, M., and K. N. Buck. 2012. The organic complexation of iron in the marine environment: A review. Front. Microbiol. **3**: 69. doi:10.3389/fmicb.2012.00069

Granger, J., D. M. Sigman, J. A. Needoba, and P. J. Harrison. 2004. Coupled nitrogen and oxygen isotope fractionation of nitrate during assimilation by cultures of marine phytoplankton. Limnol. Oceanogr. **49**: 1763–1773. doi:10.4319/lo.2004.49.5.1763

Granger, J., and D. M. Sigman. 2009. Removal of nitrite with sulfamic acid for nitrate N and O isotope analysis with the denitrifier method. Rapid Commun. Mass Spectrom. **23**: 3753–3762. doi:10.1002/rcm.4307

Hernández-de-la-Torre, B., G. Gaxiola-Castro, S. Alvarez-Borrego, J. Gómez-Valdés, and S. Nájera-Martínez. 2003. Interannual variability of new production in the southern region of the California current. Deep-Sea Res. Part II Top. Stud. Oceanogr **50**: 2423–2430. doi:10.1016/S0967-0645(03)00129-2

Hogle, S. L., and others. 2018. Pervasive iron limitation at subsurface chlorophyll maxima of the California current. Proc. Natl. Acad. Sci. USA **115**: 13300–13305. doi:10.1073/pnas.1813192115

Hutchins, D. A., and K. W. Bruland. 1998. Iron-limited diatom growth and Si:N uptake ratios in a coastal upwelling regime. Nature **393**: 561–564. doi:10.1038/31203

Jacox, M. G., J. Fiechter, A. M. Moore, and C. A. Edwards. 2015. ENSO and the California current coastal upwelling response. J. Geophys. Res. Ocean. **120**: 1691–1702. doi:10.1002/2014JC010650

Jacox, M. G., E. L. Hazen, K. D. Zaba, D. L. Rudnick, C. A. Edwards, A. M. Moore, and S. J. Bograd. 2016. Impacts of the 2015-2016 El Niño on the California current system: Early assessment and comparison to past events. Geophys. Res. Lett. **43**: 7072–7080. doi:10.1002/2016GL069716

Kahru, M., R. Kudela, M. Manzano-Sarabia, and B. G. Mitchell. 2009. Trends in primary production in the California current detected with satellite data. J. Geophys. Res. Ocean. **114**: 1-7. doi:10.1029/2008JC004979

Kelly, T. B., R. Goericke, M. Kahru, H. Song, and M. R. Stukel. 2018. CCE II: Spatial and interannual variability in export efficiency and the biological pump in an eastern boundary current upwelling system with substantial lateral advection. Deep-Sea Res. Part I Oceanogr. Res. Pap **140**: 14–25. doi:10.1016/j.dsr.2018.08.007

King, A. L., and K. Barbeau. 2007. Evidence for phytoplankton iron limitation in the southern California current system. Mar. Ecol. Prog. Ser. **342**: 91–103. doi:10.3354/meps342091

King, A. L., K. N. Buck, and K. A. Barbeau. 2012. Quasi-Lagrangian drifter studies of iron speciation and cycling off point conception, California. Mar. Chem **128–129**: 1–12. doi:10.1016/j.marchem.2011.11.001

Kirchman, D. L., B. Meon, M. T. Cottrell, D. A. Hutchins, D. Weeks, and K. W. Bruland. 2000. Carbon versus iron limitation of bacterial growth in the California upwelling regime. Limnol. Oceanogr. **45**: 1681–1688. doi:10.4319/lo.2000.45.8.1681

Lampe, R. H., E. L. Mann, N. R. Cohen, and others. 2018. Different iron storage strategies among bloom-forming diatoms. Proceedings of the National Academy of Sciences. **115**: E12275–E12284. doi:10.1073/PNAS.1805243115

Laperriere, S. M., M. Morando, D. G. Capone, T. Gunderson, J. M. Smith, and A. E. Santoro. 2020. Nitrification and nitrous oxide dynamics in the Southern California Bight. Limnol. Oceanogr **66**: 1099–1112. doi:10.1002/lno.11667

Lilly, L. E., U. Send, M. Lankhorst, T. R. Martz, R. A. Feely, A. J. Sutton, and M. D. Ohman. 2019. Biogeochemical anomalies at two Southern California current system moorings during the 2014–2016 warm anomaly-El Niño sequence. J. Geophys. Res. Ocean. **124**: 6886–6903. doi:10.1029/2019JC015255

Lilly, L. E., and M. D. Ohman. 2021. Euphausiid spatial displacements and habitat shifts in the southern California current system in response to El Niño variability. Prog. Oceanogr. **193**: 102544. doi:10.1016/j.pocean.2021.102544

Mantyla, A. W., S. J. Bograd, and E. L. Venrick. 2007. Patterns and controls of chlorophyll-a and primary productivity cycles in the Southern California Bight. J. Marine Syst. **73**: 48–60. doi:10.1016/j.jmarsys.2007.08.001

McClatchie, S. 2014. Regional fisheries oceanography of the California current system: The CalCOFI program. Springer. doi:10.1007/978-94-007-7223-6

McIlvin, M. R., and K. L. Casciotti. 2011. Technical updates to the bacterial method for nitrate isotopic analyses. Anal. Chem. **83**: 1850–1856. doi:10.1021/ac1028984

Nagarkar, M., M. Wang, B. Valencia, and B. Palenik. 2021. Spatial and temporal variations in *Synechococcus* microdiversity in the Southern California coastal ecosystem. Environ. Microbiol. **23**: 252–266. doi:10.1111/1462-2920.15307

Ohman, M. D., G. H. Rau, and P. M. Hull. 2012. Multi-decadal variations in stable N isotopes of California current zooplankton. Deep-Sea Res. Part I Oceanogr. Res. Pap **60**: 46–55. doi:10.1016/j.dsr.2011.11.003

Peng, X., S. E. Fawcett, N. van Oostende, M. J. Wolf, D. Marconi, D. M. Sigman, and B. B. Ward. 2018. Nitrogen uptake and nitrification in the subarctic North Atlantic Ocean. Limnol. Oceanogr. **63**: 1462–1487. doi:10.1002/lno.10784

Plattner, G.-K. 2005. Decoupling marine export production from new production. Geophys. Res. Lett. **32**: L11612. doi:10.1029/2005GL022660

Rafter, P. A., D. M. Sigman, and K. R. M. Mackey. 2017. Recycled iron fuels new production in the eastern equatorial Pacific Ocean. Nat. Commun **8**: 1100. doi:10.1038/s41467-017-01219-7

Rau, G. H., M. D. Ohman, and A. Pierrot-Bults. 2003. Linking nitrogen dynamics to climate variability off Central California: A 51 year record based on 15 N/ 14 N in CalCOFI zooplankton. Deep-Sea Res. II **50**: 2431–2447. doi:10.1016/S0967-0645(03)00128-0

Santoro, A. E., K. L. Casciotti, and C. A. Francis. 2010. Activity, abundance and diversity of nitrifying archaea and bacteria in the Central California current. Environ. Microbiol. **12**: 1989–2006. doi:10.1111/j.1462-2920.2010.02205.x

Shafiee, R. T., J. T. Snow, Q. Zhang, and R. E. M. Rickaby. 2019. Iron requirements and uptake strategies of the globally abundant marine ammonia-oxidising archaeon, Nitrosopumilus maritimus SCM1. ISME J. **13**: 2295–2305. doi:10.1038/s41396-019-0434-8

Sigman, D. M., K. L. Casciotti, M. Andreani, C. Barford, M. Galanter, and J. K. Böhlke. 2001. A bacterial method for the nitrogen isotopic analysis of nitrate in seawater and freshwater. Anal. Chem. **73**: 4145–4153. doi:10.1021/ac010088e

Sigman, D. M., J. Granger, P. J. DiFiore, M. M. Lehmann, R. Ho, G. Cane, and A. van Geen. 2005. Coupled nitrogen and oxygen isotope measurements of nitrate along the eastern North Pacific margin. Global Biogeochem. Cycles **19**: 1–14. doi:10.1029/2005GB002458

Sigman, D. M., P. J. DiFiore, M. P. Hain, C. Deutsch, and D. M. Karl. 2009. Sinking organic matter spreads the nitrogen isotope signal of pelagic denitrification in the North Pacific. Geophys. Res. Lett. **36**: 1–5. doi:10.1029/2008GL035784

Sigman, D. M., and F. Fripiat. 2019. Nitrogen isotopes in the ocean, p. 263–278. *In* Encyclopedia of ocean sciences. Elsevier. doi:10.1016/B978-0-12-409548-9.11605-7

Smart, S. M., S. E. Fawcett, S. J. Thomalla, M. A. Weigand, C. J. C. Reason, and D. M. Sigman. 2015. Isotopic evidence for nitrification in the Antarctic winter mixed layer. Global Biogeochem. Cycles **29**: 427–445. doi:10.1002/2014GB005013

Smith, J. M., F. P. Chavez, and C. A. Francis. 2014. Ammonium uptake by phytoplankton regulates nitrification in the Sunlit Ocean. PLoS One **9**: e108173. doi:10.1371/journal.pone.0108173

Stephens, B. M., M. Porrachia, S. Dovel, M. Roadman, R. Goericke, and L. I. Aluwihare. 2018. Nonsinking organic matter production in the California current. Global Biogeochem. Cycles **32**: 1386–1405. doi:10.1029/2018GB005930

Stephens, B. M., S. D. Wankel, J. M. Beman, A. J. Rabines, A. E. Allen, and L. I. Aluwihare. 2019. Euphotic zone nitrification in the California current ecosystem. Limnol. Oceanogr. **65**: 790–806. doi:10.1002/lno.11348

Strzepek, R. F., P. W. Boyd, and W. G. Sunda. 2019. Photosynthetic adaptation to low iron, light, and temperature in Southern Ocean phytoplankton. Proc. Natl. Acad. Sci. USA **116**: 4388–4393. doi:10.1073/pnas.1810886116

Stukel, M. R., M. R. Landry, C. R. Benitez-Nelson, and R. Goericke. 2011. Trophic cycling and carbon export relationships in the California current ecosystem. Limnol. Oceanogr. **56**: 1866–1878. doi:10.3354/meps010257

Stukel, M. R., and K. A. Barbeau. 2020. Investigating the nutrient landscape in a coastal upwelling region and its relationship to the biological carbon pump. Geophys. Res. Lett. **47**: e2020GL087351. doi:10.1029/2020GL087351

Sugimoto, R., A. Kasai, T. Miyajima, and K. Fujita. 2009. Controlling factors of seasonal variation in the nitrogen isotope ratio of nitrate in a eutrophic coastal environment. Estuar. Coast. Shelf Sci. **85**: 231–240. doi:10.1016/J.ECSS.2009.08.006

Tems, C. E., W. M. Berelson, and M. G. Prokopenko. 2015. Particulate δ15N in laminated marine sediments as a proxy for mixing between the California undercurrent and the California current: A proof of concept. Geophys. Res. Lett. **42**: 419–427. doi:10.1002/2014GL061993

Turk-Kubo, K. A., M. M. Mills, K. R. Arrigo, G. van Dijken, B. A. Henke, B. Stewart, S. T. Wilson, and J. P. Zehr. 2021. UCYN-A/haptophyte symbioses dominate N2 fixation in

the Southern California current system. ISME Commun. **1**: 42. doi:10.1038/s43705-021-00039-7

Wankel, S. D., C. Kendall, J. T. Pennington, F. P. Chavez, and A. Paytan. 2007. Nitrification in the euphotic zone as evidenced by nitrate dual isotopic composition: Observations from Monterey Bay, California. Global Biogeochem. Cycles **21**: GB2009. doi:10.1029/2006GB002723

Ward, B. 2005. Temporal variability in nitrification rates and related biogeochemical factors in Monterey Bay, California, USA. Mar. Ecol. Prog. Ser **292**: 97–109. doi:10.3354/meps292097

Ward, B. B., and A. F. Carlucci. 1985. Marine ammonia- and nitrite-oxidizing bacteria: Serological diversity determined by immunofluorescence in culture and in the environment. Appl. Environ. Microbiol. **50**: 194–201. doi:10.1128/aem.50.2.194-201.1985

Ward, B. B., H. E. Glover, and F. Lipschultz. 1989. Chemoautotrophic activity and nitrification in the oxygen minimum zone off Peru. Deep-Sea Res. Part A. Oceanogr. Res. Pap **36**: 1031–1051. doi:10.1016/0198-0149(89)90076-9

Weigand, M. A., J. Foriel, B. Barnett, S. Oleynik, and D. M. Sigman. 2016. Updates to instrumentation and protocols for isotopic analysis of nitrate by the denitrifier method. Rapid Commun. Mass Spectrom. **30**: 1365–1383. doi:10.1002/RCM.7570

Wohlers, J., A. Engel, E. Zöllner, P. Breithaupt, K. Jürgens, H. G. Hoppe, U. Sommer, and U. Riebesell. 2009. Changes in biogenic carbon flow in response to sea surface warming. Proc. Natl. Acad. Sci. USA **106**: 7067–7072. doi:10.1073/PNAS.0812743106/SUPPL_FILE/0812743106SI.PDF

Yool, A., A. P. Martin, C. Fernández, and D. R. Clark. 2007. The significance of nitrification for oceanic new production. Nature **447**: 999–1002. doi:10.1038/nature05885

Acknowledgments

The authors would like to thank the technicians and crew of the CalCOFI program, and Shonna Dovel in particular for sample collection. They would also like to thank Zoe Sandwith and Jennifer Karolewski for helping with NO_3^- isotope analyses and Yury Kiselev for helping with data analysis. They also thank Daniel Sigman and the Sigman Lab at Princeton University for assistance with sample analysis and two anonymous reviewers for improving the manuscript. Datasets presented here were supported in part by CCE-LTER augmented funding (NSF grant OCE-1026607). Additional funding came from the Edna Bailey Sussman Foundation and NSF grant OCE-1736656.

Conflict of Interest

None declared.

Submitted 26 March 2021
Revised 14 October 2021
Accepted 25 June 2022

Associate editor: Phyllis Lam